ACOUSTIC SCATTERING FROM AN OBJECT IN A MUD LAYER OF A SHALLOW WATER WAVEGUIDE

Steven G. Kargl, Kevin L. Williams, Aubrey L. Espana

Applied Physics Laboratory, University of Washington, 1013 NE 40th St., Seattle WA 98105-6698 USA

Steven G. Kargl, Applied Physics Laboratory, University of Washington, 1013 NE 40th St., Seattle WA 98105-6698 USA, FAX: 206-543-1300, kargl@uw.edu

Abstract: *Bay Experiment 2014 (BAYEX14) collected low-frequency synthetic aperture sonar (SAS) data in St. Andrew's Bay, Panama City, FL. Inert ordnance, scientific targets, and some clutter objects were distributed in the field of view of the SAS system. The environment is roughly characterized by a 7-m water depth with a mud layer over a sand sediment subbottom. The layer thickness varies from 15 to 30 cm. All objects deployed in BAYEX14 sank into the mud layer. Large targets were partially buried and came to rest on the underlying sand sediment; while small targets were completely buried. Modifications to the APL-UW target in the environment response (TIER) model were required to account for propagation paths within the mud layer. Simulations and comparisons to BAYEX14 data suggest that the primary contribution to the received scattered signal is the direct scattering ray path. The SAS platform was near the middle of the water column. For objects with horizontal ranges from the SAS platform that exceed a few water depths, an air-water reflected ray path can significantly alter the scattered signal and, under calm conditions, ocean surface bounce target images can be formed. These topics will be the focus of this paper. [Work supported by SERDP and ONR.]*

Keywords: *Synthetic aperture sonar, Unexploded ordnance, mud layer.*

1. INTRODUCTION

Although disposal of munitions in coastal waters was discontinued during the 1970's, environmental, economical, and recreational impact persist [1]. Overfield and Symons note that over 2100 underwater sites are likely to contain shipwrecks, munitions dumpsites, radiological waste, abandoned pipelines, and wellheads [2]. Of those sites, verification has been completed on approximately 50% with contemporary records (e.g., ship logs). Although not all sites listed in the Resources and Undersea Threats (RUST) database contain discarded munitions, RUST also may not contain a comprehensive list of current and former US military training sites. In any event, there is a clear need for cost-effective surveys of underwater sites. Schwartz and Brandenburg summarize the current technologies available for underwater unexploded ordnance (UXO) applications [3]. Their Table 1 includes chemical sensors, metal detection, and sonar. Chemical sensors and metal detection are typically restricted to very short ranges; while sonar technologies considered in [3] are limited in range or are limited by poor penetration into sediments due to the sonar's high frequency.

Low-frequency (LF) sonar in underwater UXO remediation activities has been considered by researchers at the Naval Research Laboratory [4,5] and by our group at the Applied Physics Laboratory, University of Washington (APL-UW) [6-10]. Sound below 50 kHz has three advantages. First, it can propagate to hundreds of meters with little attenuation loss. Second, low frequencies can penetrate into sediments, and have the potential to detect buried objects. Third, and importantly, low frequencies can couple into an elastic response of an object. This response can then be utilized in classification schemes.

Much of our previous efforts focused on LF synthetic aperture sonar (SAS) to ensonify underwater objects resting on a water-sediment interface. Field experiments with numerous objects (including inert UXO, scientific targets, and clutter objects) have been conducted. Data were used to validate finite-element (FE) models and a fast ray-based model [6-10]. This research demonstrated that the environment within which an object is found must be considered when determining its elastic response. Combining acoustic scattering amplitudes from FE simulations with the fast ray-model has led to the target-in-the-environment-response (TIER) model. When an object becomes buried within a sediment, the TIER model requires modifications. During Bay Experiment 2014 (BAYEX14), all targets were partially or fully buried in a thin mud layer above a sandy subbottom. This paper discusses modifications to the TIER model to account for propagation under BAYEX14 conditions. Section 2 describes BAYEX14. Section 3 outlines the TIER model and discusses the modifications required to account for propagation within the mud layer. Section 4 provides simulations that show the mud layer's effect on an object's response and effects of an air-water reflected path. Section 5 summarizes.

2. BAY EXPERIMENT 2014

BAYEX14 was conducted in St. Andrew's Bay, Panama City, FL in late Spring of 2014. The environment is characterized by a 7 to 8 m water depth with a mud layer over a sandy subbottom. The thickness of the mud layer varies from 15 to 30 cm. The water in the bay is brackish due to tidal exchange and inflow of freshwater. This environment provided two unique situations not encountered in our previous field measurements; namely, the mud layer and the air-water interface could not be ignored under certain conditions.

The *Research Vessel (RV) Sharp* was placed in a four-point moor with a westward heading. APL-UW's rail-tower sonar platform was deployed parallel to the *RV Sharp* off her starboard side. The rail provided a 40-m SAS aperture with target fields placed north of the

rail in the field-of-view of the sonar. The tower moved along the rail at 5 cm/s, and simultaneously transmitted 1-30 and 110-190 kHz linear-frequency-modulated (LFM) pulses with a 2 Hz repetition frequency.

Divers installed a fixed grid of lightweight cords from 5 to 40 m in 5 m intervals. Objects were placed at grid locations with specified orientations. Adjacent objects have sufficient separation such that multiple scattering can be ignored. A target field could contain 10 to 28 objects during the collection of SAS data. All objects deployed in BAYEX14 sank into a mud layer coming to rest on a sandy subbottom. Large objects were partially buried; while small objects were completely buried. The source and receiver were located approximately 3.8 m above the subbottom, which coincided with the nominal mid column of the waveguide. With this source/receiver location and under calm conditions an air-water reflected acoustic path can contribute to the measured acoustic scattered pressure. Thus, the mud layer and shallow water environment posed new requirements on our TIER model.

3. MODIFIED TIER MODEL

When the depth of a homogeneous waveguide is much larger than a wavelength of sound, the Green function for propagation can be represented by a superposition of image sources reflected through the waveguide's boundaries. Likewise, a receiver in the waveguide can be represented by a superposition of image receivers. The TIER model utilizes image sources and receivers to represent the propagation associated with acoustic scattering from an object within a waveguide. A detailed description of the TIER model is available in [7]. Here, we simply give a brief description.

With r_i, r_j, and r_t representing source, receiver, and object locations, the physical source (receiver) corresponds to $i = 0$ ($j = 0$) and its images have $i > 0$ ($j > 0$). The distance between a source and object is $d_{ti} = |r_t - r_i|$, and $d_{jt} = |r_j - r_t|$ is the distances between a receiver and object. The propagation time delay along the ray joining a source and object is $t_{ti} = d_{ti} / c_1$, and the time delay for the object to receiver is $t_{jt} = d_{jt} / c_1$. The sound speed in water is c_1. The total scattering pressure is then the superposition of contributions of form:

$$P_{ij}(\omega) = \left[\frac{A_{jt}}{d_{jt}}\exp(i\omega t_{jt})\right]\left[\frac{A_{ti}}{d_{ti}}\exp(i\omega t_{ti})\right] f(k_i, k_j, \omega) r_0 P_{src}(\omega). \quad (1)$$

A_{jt} and A_{ti} account for source and receiver beam patterns and any interaction of a ray with the boundaries of the waveguide. In (1), the scattering process is a multiplication of the free-field scattering amplitude, $f(k_i,k_j,\omega)$, with the spectrum of the transmitted pulse, $P_{src}(\omega)$. The incident and scattered wave vectors, associated with source i and receiver j, are k_i and k_j, respectively. These wave vectors are defined within a target-centered coordinate geometry. Finally, r_0 is a reference distance associated with calibration of the source.

The distance between the actual source and actual receiver on the APL-UW sonar platform is much smaller than the slant range to an object, so the source and receiver are assumed to be co-located. In our experiments prior to BAYEX14, the air-water interface can be ignored, because rays that interact with this interface are removed by time-gating the received signals (see below). Under these conditions, only four rays contribute to the total scattered pressure. With S, R, T, and B denoting the source, receiver, target, and bottom, the 4 rays are given by S→T→R (direct scattering path), S→B→T→R and S→T→B→R (reciprocal paths with one bottom bounce), and S→B→T→B→R (double bounce path). The arrow denotes direction of propagation. The conditions of BAYEX14 [10] required modifications to the TIER model.

Consider a uniform layer bounded above by water and below by a homogeneous subbottom. Assume a layer thickness of h and an origin of the coordinate system in the interface separating the layer and subbottom. The layer permits additional ray paths to reach

an object. For a source (or receiver) at a finite horizontal range R from an object within the layer, refracted ray paths exist and satisfy

$$(z_s - h)\cot\theta_{m,1} + mh\cot\theta_{m,2} + (h - z_t)\cot\theta_{m,2} - R = 0\,, \qquad m \text{ even}, \tag{2}$$

$$(z_s - h)\cot\theta_{m,1} + mh\cot\theta_{m,2} + z_t\cot\theta_{m,2} - R = 0\,, \qquad m \text{ odd}, \tag{3}$$

where z_s and z_t are the z coordinates of the source and object. The integer m enumerates the number of internal reflections within the layer. That is, path 0 crosses the water-layer interface, but otherwise does not interact with a boundary; while path 1 reflects once from the layer-subbottom interface (see Fig. 1). To describe the scattering process, it is convenient to write 0→1 to mean an incident path 0 is scattered into an outgoing path 1. For ray m, an incident grazing angle $\theta_{m,1}$ is related to an angle of refraction $\theta_{m,2}$ via Snell's laws, $\cos\theta_{m,2} = \nu \cos\theta_{m,2}$, where the real index of refraction is $\nu = c_1 / c_2$. The speed of sound in the layer is c_2. Snell's law allows one to eliminate $\theta_{m,2}$ from (2) and (3), and then solve the resulting transcendental equation for $\theta_{m,1}$. The length of a ray's path within the water is

$$d_{m,1} = (z_s - h)\csc\theta_{m,1}, \tag{4}$$

and the total length of a ray's path in the layer is

$$d_{m,2} = (mh - z_t + h)\csc\theta_{m,2}, \qquad \text{m even}, \tag{5}$$

$$d_{m,2} = (mh + z_t)\csc\theta_{m,2}, \qquad \text{m odd}, \tag{6}$$

Finally, mud has a fairly high acoustic absorption in comparison to water. For that portion of a ray path in mud, the absorption loss is given by

$$loss_{m,2} = \exp(-\delta d_{m,2}\omega / c_2)\,, \tag{7}$$

where δ is a dimensionless loss parameter.

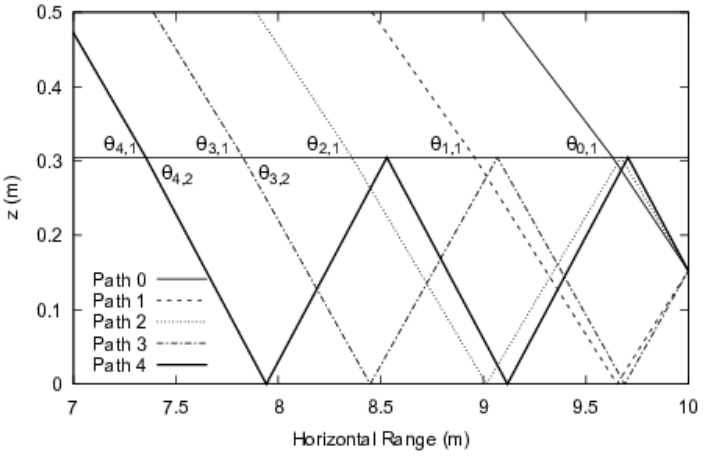

Fig. 1. Five ray paths for a BAYEX14 simulation with an object at a 10 m horizontal range. The layer-subbottom interface is at z = 0. The horizontal black line indicates the water-layer interface. Physical properties of mud are close to those of water, so the ray paths are only slightly refracted crossing the water-layer interface. For clarity, refraction angles $\theta_{0,2}$, $\theta_{1,2}$, and $\theta_{2,2}$ have been omitted.

4. MODEL-DATA COMPARSION

In BAYEX14, the speeds of sound in water and mud were c_1= 1530 m/s and c_2 = 1504 m/s, respectively. For mud, the loss parameter, δ, is typically in the range of 0.01 to 0.02. A solid aluminum cylinder (2 ft length by 1 ft diameter) was placed at a horizontal range of R = 20 m where the layer thickness is $h \approx 0.16$ m. Co-located source/receiver heights are z_s = 3.8 m and

the target center has z_t = 0.1524 m. As a ray propagates in the layer, acoustic energy is absorbed by the layer. Using (5) - (7) with δ = 0.01, one-way absorption losses for individual paths are shown in Table 1.

m	$\theta_{m,1}$ (deg)	$d_{m,1}$ (m)	$d_{m,2}$ (m)	dB 1 kHz	dB 10 kHz	dB 20 kHz	dB 30 kHz
0	10.33	20.30	0.030	-0.01	-0.11	-0.22	-0.33
1	10.93	19.20	1.194	-0.43	-4.33	-8.67	-13.00
2	10.96	19.14	1.250	-0.45	-4.54	-9.07	-13.61
3	11.59	18.11	2.345	-0.85	-8.51	-17.02	-25.53
4	11.62	18.06	2.398	-0.87	-8.70	-17.40	-26.10

Table 1. One-way absorption loss in mud for rays to those depicted in Fig. 1. The last four columns contain the loss at the specified frequency. Note, this loss does not account for reflection and transmission coefficients at the lower and upper boundaries of the layer.

The target strength (TS) for the aluminum cylinder under different environmental conditions is displayed in Fig. 2. The simulation conditions are those that match the above BAYEX14 conditions with the cylinder at R = 20 m. Fig. 2a and 2c correspond to a broadside orientation of the cylinder while Fig. 2b and 2d are for an end-on orientation. The free-field result (black line) is the direct scattering in the absence of any boundaries (i.e., S→T→R). The blue line in Fig. 2a and 2b is the scattering from the cylinder sitting proud on the subbottom in the absence of a mud layer. The green, red, and cyan lines in Fig. 2a and 2b are the TS for the cylinder in the mud layer with δ = 0.00, 0.01, and 0.02, respectively. In Fig. 2c and 2d, the 0→0, 0→1 + 1→0, and 1→1 ray contributions to the TS for a cylinder in the mud

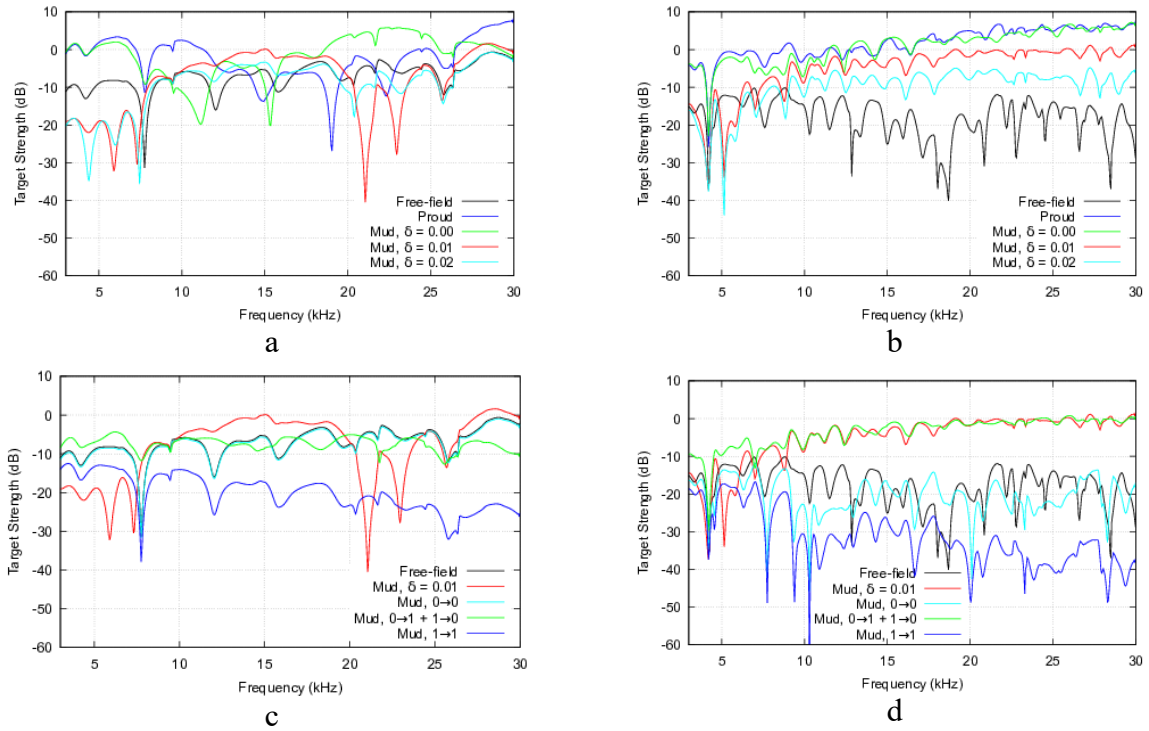

Fig. 2. TIER model TS simulations of the scattering from a 2:1 solid aluminum cylinder: a. cylinder in broadside orientation; b. cylinder in end-on orientation; c. broadside orientation for free-field scattering and scattering in mud layer with δ = 0.01; and, d. end-on orientation for free-field scattering and scattering in mud layer with δ = 0.01. Individual path contributions 0→0, 0→1 + 1→0, and 1→1 are also shown in c and d.

layer are depicted. This allows one to see the significance of 0→0, 0→1 + 1→0, and 1→1 contributions, and shows the frequency dependence of the absorption loss (e.g., the 1→1 path is significantly lower than the 0→1 + 1→0 paths).

In the shallow water environment of BAYEX14 with objects deployed to a 40 m horizontal range and source/receiver near the middle of the water column, reflections from the air-water interface are unavoidable for the type of broad beamwidth transducers used in BAYEX14. In the following TIER simulations, we ignore the mud layer and consider the superposition of $P_{ij}(\omega)$ as given in (1) with $i_{max} = j_{max} = 1$ and $i_{max} = j_{max} = 2$. The former case is a simulation for the four ray paths S→T→R, etc. with an image source and image receiver below the water-sediment interface. The latter case includes nine contributions where an additional image source and image receiver occur above the air-water interface. The simulations are for a 3:1 aluminum cylinder at the centre of a circular SAS (CSAS) path. A CSAS simulation allows the TIER model to generate a full 360° acoustic colour (AC) template (i.e., TS as a function of aspect angle and frequency) with a single simulation. The transmitted LFM pulse spans 1-30 kHz with a pulse duration of 6 ms. Fig. 3 shows the TIER model results for the simulations with the cylinder at the centre of CSAS paths with 10 and 40 m radii. Here, the time signals have been pulse compressed. The red box denotes that portion of the time signals used in the construction of SAS images and AC templates. Column b shows that the air-water interface contributions can be time-gated out; while column d shows an unavoidable

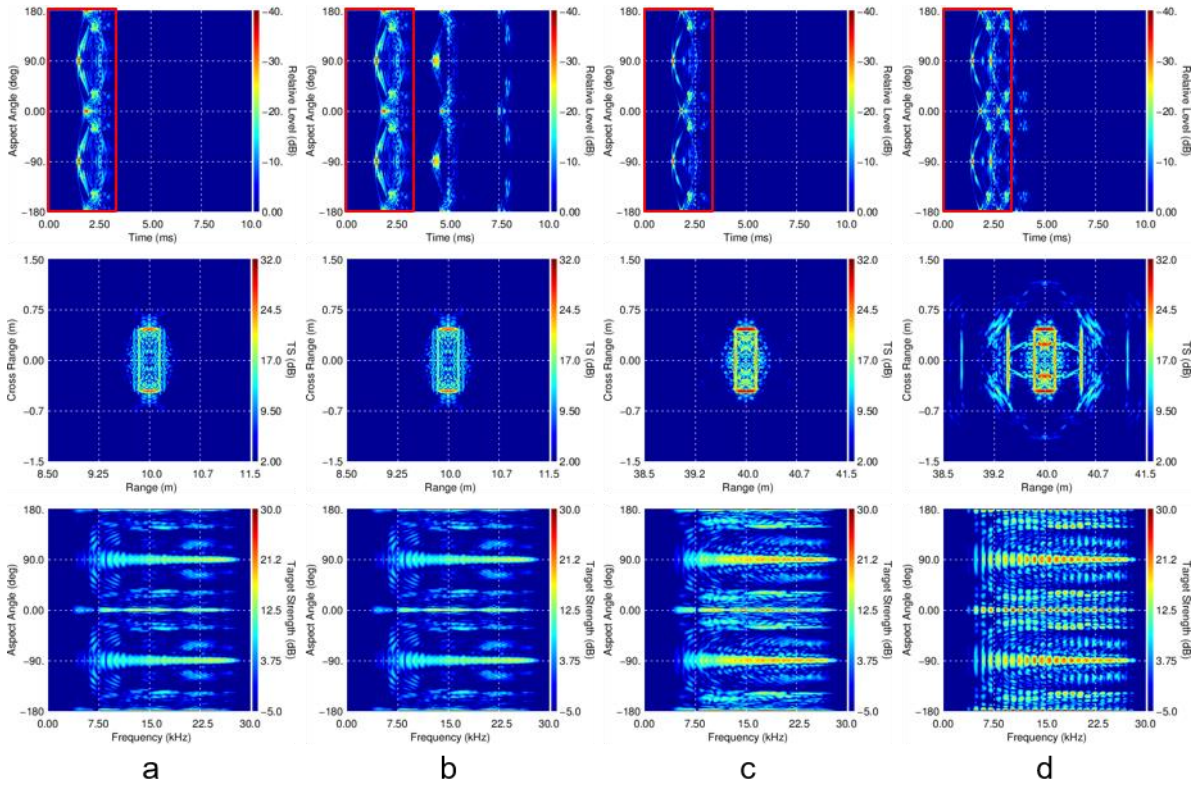

Fig. 3. CSAS TIER simulations for 3:1 aluminum cylinder. Columns a and b are for a 10 m radius CSAS path. Columns c and d are for 40 m radius CSAS path. Columns a and c have $i_{max} = j_{max} = 1$. Columns b and d have $i_{max} = j_{max} = 2$. Top row is the pulse-compressed scattered signals. Middle row is the SAS images constructed from the portion of the time signals in the red box. Bottom row is the AC templates for the portion of time signals in the red box.

overlap of air-water interface contributions within the time window of interest. This overlap causes what appear to be artefacts in the SAS image (column d, middle). The coherent SAS processing that focuses the $i_{max} = j_{max} = 1$ data does not properly account for the propagation

phase delay associated with the image source and image receiver above the air-water interface. Inspection of the time signals in Fig 3 (column b and d) reveals that the late-time arrivals from the air-water interface have a constant lag. Instead of constructing a SAS image from the primary returns at a reference distance, R, associated with the actual source/receiver location, the air-water arrivals can be used to construct a focused image at reference distance associated with the image source/receiver in air, $R + c_1 \times \text{lag}$. When these time-domain data are converted into a AC template, it is observed that the air-water interface contribution causes a modulation in the TS (see Fig. 3d, bottom). AC templates are often used in classification schemes. If a lack of recognition of the modulation exists during training and/or testing, then classification likely may fail for an object in shallow water.

5. SUMMARY

Inspection of Table 1 and Fig. 2 reveals that for objects placed at horizontal ranges that exceed a few water depths, the upper portion of the frequency band of the LF LFM pulse is extensively attenuated. The scattering amplitude in (1) determines the directionality of the scattered acoustic field. For co-located source/receiver, this means for an incident acoustic field that propagates along say path 0 in Fig. 1, a portion of its acoustic energy may be scattered into paths 0, 1, 2, … For the case of a nominally half-buried cylinder, the free-field result and 0→0 are nearly identical at broadside (see Fig. 2c) and have the same general level in an end-on orientation (see Fig. 2d). More importantly, Table 1 suggests that paths with multiple internal reflections become insignificant through absorption loss. It is also observed that for a given path length in the mud layer, high frequencies suffer significant absorption loss. This then yields reduced effective bandwidth of the LFM pulse, which degrades SAS image resolution.

A shallow water environment can impact the SAS image and the AC template for an object that is placed several water depths in horizontal range from the SAS platform, because air-water interface reflected paths can contribute under calm conditions. For BAYEX14, the water depth is about 8 m with broad-beamwidth source and receiver near mid-column. For objects in the 25 to 40 m horizontal range, SAS images display artefacts and AC templates show a modulation.

6. ACKNOWLEDGEMENTS

The research reported was jointly funded by the Strategic Environmental Research and Development Program (SERDP) and the Office of Naval Research (ONR). BAYEX14 was conducted in collaboration with the Naval Surface Warfare Center, Panama City Division.

REFERENCES

[1] **TP Long**, A global prospective on underwater munitions, *Mar. Technol. Soc. J.*, 43, pp. 5-10, 2009.

[2] **ML Overfield, LC Symons**, The use of the RUST database to inventory, monitor, and assess risk from Undersea Threats, *Mar. Technol. Soc. J.*, 43, pp. 33-40, 2009.

[3] **A Schwartz, E Brandeburg**, An overview of underwater technologies for operations involving underwater munitions, *Mar. Technol. Soc. J.*, 43, pp. 62-75, 2009.

[4] **JA Bucaro, BH Houston, M Saniga, LR Dragonette, T Yoder, S Dey, L Kraus, L Carin**, Broadband acoustic scattering measurements of underwater unexploded ordnance (UXO), *J. Acoust. Soc. Am.*, 123, pp. 738-746, 2008.

[5] **JA Bucaro; H Simpson, L Kraus, LR Dragonette, T Yoder, BH Houston**, Bistatic scattering from submerged unexploded ordnance lying on a sediment, *J. Acoust. Soc. Am.,* 126, pp. 2315-2323, 2009.

[6] **SG Kargl, KL Williams, TM Marston, JL Kennedy, JL Lopes**, Acoustic response of unexploded ordnance (UXO) and cylindrical targets, in *Proc. OCEANS 2010 MTS/IEEE*, Seattle WA, pp. 6, DOI: 10.1109/OCEANS.2010.5664392.

[7] **SG Kargl, AL Espana, KL Williams, JL Kennedy, JL Lopes**, Scattering from objects at a water sediment interface: Experiment, high-speed and high-fidelity models, and physical insight, *IEEE J. Ocean. Eng*., 40, pp. 632-642, 2015.

[8] **M Zampolli, AL Espana, KL Williams, SG Kargl, EI Thorsos, JL Lopes, JL Kennedy**, **PL Marston**, Low- to mid-frequency scattering from elastic objects on a sand sea floor: Simulation of frequency and aspect dependent structural echoes, *J. Comp. Acoust*., 20, p. 1240007 (14 pp.), 2012, DOI: 10.1142/S0218396X12400073.

[9] **KL Williams, SG Kargl, EI Thorsos, DS Burnett, JL Lopes, M Zampolli, PL Marston**, Acoustic scattering from a solid aluminum cylinder in contact with a sand sediment: Measurements, modeling, and interpretation, *J. Acoust. Soc. Am*., 127, pp. 3356-3371, 2010.

[10] **KL Williams,** Buried targets in layered media: A combined finite element/physical acoustics model and comparison to data on a half buried 2:1 cylinder, *J. Acoust. Soc. Am*., 140, EL504 (2016); https://doi.org/10.1121/1.4971324